Angew. Chem. Int. Ed. 50 (2011) 10226-10230

Oxygen Insertion Catalysis by sp^2 Carbon

B. Frank, R. Blume, A. Rinaldi, A. Trunschke*, R. Schlögl

Department of Inorganic Chemistry, Fritz Haber Institute of the Max Planck Society,
Faradayweg 4-6, 14195 Berlin, Germany

* Corresponding author: e-mail trunschke@fhi-berlin.mpg.de,

Received 13 May 2011; Revised 9 June 2011; Published online 16 August 2011

Abstract

Black matter in catalysis: Graphitic carbon catalyzes the insertion of O atoms into acrolein. Such complex multistep atom rearrangements were believed to be the exclusive domain of metal (oxide) catalysis. In the C-catalyzed process, the nucleophilic O atoms terminating the graphite (0001) surface abstract the formyl H atom and the activated aldehyde is oxidized by a mobile epoxide O atom. Thus, the sp^2 carbon acts as a bifunctional catalyst.

Keywords: aldehydes; carbocatalysis; C-H activation; graphite; oxygen

Dedicated to the Fritz Haber Institute, Berlin, on the occasion of its 100th anniversary

1. Introduction

Elemental carbon with sp^2 hybridization is omnipresent in our lives and in its natural form graphite an integral part of pencils, batteries, lubricants, steel, or electric motor brushes. High-tech electronic devices or the neutron moderators in nuclear power plants are made of synthetic graphite with a low defect density – the amount of carbon atom dislocations in the hexagonal lattice. Nanostructured sp^2 carbon is used as a pigment (carbon black) and as polymer filler. The discovery and synthesis of non-planar carbon allotropes, such as CNTs or fullerenes,[1] ushered in a new era of cutting-edge applications for elemental carbon. The basic structural unit (BSU) is graphene[2] with edge defects and curvature induced by non-six-membered carbon rings.

In chemical sciences, graphitic forms of carbon display an intriguing potential in catalysis with a broad application area covering hydrogenation, oxidation, polymerization, or chlorination reactions.[3,4] The increased reaction scope in view has recently been reviewed by Dreyer and Bielawski,[5] who themselves investigated the catalytic activity of graphene oxide for several reactions under mild reaction conditions in liquid phase.[6] As the most prominent example for *gas* phase heterogeneous catalysis by carbon materials, nucleophilic oxygen atoms located at the prismatic edges of stacked graphene sheets or at surface defects in the (0001) graphitic surface selectively catalyze the oxidative dehydrogenation (ODH) of ethylbenzene to styrene [7,8], a reaction of high industrial relevance. For the oxygen-free pathway (DH), the activity of nanocrystalline diamonds coated with defective graphene shells, so-called bucky diamonds, even exceed the industrial K-promoted Fe catalyst.[9] It is not surprising that the ODH of the light alkanes suffers from a by far lower selectivity due to the weaker C–H bond strength in the product molecule as compared to the substrate [10] – a common problem in selective oxidation reactions.[11] Point defects filled with electrophilic oxygen likely initiate non-selective combustion pathways. The low-dimensionality of nanostructured carbon materials offers the possibility to modify and optimize the chemical environment of active sites in a unique quality, thus obtaining rigid structure-reactivity correlations. The absence of strongly Lewis-acidic metal cations minimizes coke deposition and thus catalyst deactivation, which can in turn reduce process costs by omitting the addition of steam or periodical catalyst regeneration by coke burning.[9]

Such progress in ODH and DH catalysis encouraged us to test nanostructured carbon catalysts in the gas-phase selective oxidation of acrolein to acrylic acid (AA) as the model reaction for oxygen insertion (Eq. 1).

$$CH_2{=}CH{-}CHO + \tfrac{1}{2}\,O_2 \rightarrow CH_2{=}CH{-}COOH \qquad (1)$$

Here, the H abstraction from the formyl group is followed by oxygenation to form the carboxyl functionality. This reaction is industrially realized over optimized Mo/V mixed metal oxide catalysts providing AA yields of >95% at temperatures as low as 200–300°C.[12] The addition of steam to the feed increases the performance and life-time of the catalysts [12-14]. Graphitic carbon allotropes can resist the oxidative stress under these conditions.[15] However, natural graphite flakes applied as the heterogeneous catalyst for this reaction show a poor C_3H_4O conversion of 0.4% at an AA selectivity of only 37%. The comparison of graphite flakes of different diameter discloses the location of the active sites: when decreasing the size of the flakes by use of ball-milled synthetic graphite, the conversion increases to 8.8% while keeping the selectivity at the moderate level of 66% pointing at the prismatic edges of stacked graphene layers as the host for the active moieties for this reaction. A pronounced evolution of the catalytic performance is observed and an initial decay of activity accompanied by an increasing selectivity during the initial 12 h time-on-stream can be related to the (trans)formation of oxygen surface species on the carbon surface (Fig. S1) and healing of point defects. Similar to (bulk) metal oxides the switch between reduced and oxidized state during the reaction will be realized by consecutive reoxidation with gas phase oxygen. However, in contrast to metal oxides and the related Mars-van Krevelen redox mechanism, the bulk of the graphite catalyst cannot serve as a reservoir for oxygen atoms. Instead, the (0001) graphitic surface, mediating the dissociative adsorption of oxygen in the carbon combustion,[16] could take on this role as well as serve as an electron buffer to facilitate the redox process at the active sites. However, the AA formation rate of 86.5 µmol g^{-1} h^{-1} for the natural graphite is unquestionably poor as compared to the industrial and academic state of the art.[12,17]

Table 1. Structural data and catalytic performance of various carbon allotropes in the selective oxidation of acrolein to acrylic acid.

Nanocarbon	S_{BET} / m^2 g^{-1}	d [a] / nm	$X(C_3H_4O)$[b] / %	$S(AA)$[b] / %
Natural graphite	11.0	123	0.4	37
Synthetic graphite	349	6	8.8	66
MWCNT	541	9.9	14	85
Fishbone CNF	50	15–20	1.8	35
OLC	315	5–15	4.5	75
Nanodiamond	1.7	5–15	3	51
Fullerenes	320	0.7	31[c]	41[c]
MCT	5.0	-	5	12
Activated carbon	835	-	26[c]	51[c]

[a] Characteristic diameter of the nanostructured carbon as determined by HRTEM, XRD for natural graphite (L_a), and Raman analysis for synthetic graphite (L_a); [b] Determined after 15 h time-on-stream; 5 vol.% C_3H_4O/10 vol.% O_2/He, 300°C, 3000 h^{-1}; side products are CO, CO_2 and trace amounts of acetic acid; [c] No stable performance due to severe oxidative degradation (C balance > 100%).

The screening of low-dimensional carbon allotropes[18] gives insight into basic structure-activity relationships (Tables 1 and S1). The superior performance is observed for the allotropes with bent graphene sheets, i.e., the multiwalled carbon nanotubes (MWCNTs) and onion-like carbon (OLC), whereas the sp^3 hybridized nanodiamonds suffer from a low AA selectivity. Disordered forms of carbon, such as activated carbon, cannot coordinate the selective reaction and, in addition, rapidly deactivate due to oxidative degradation.[15] The rapid activity loss is also observed for the C_{60} fullerenes, probably with open cage structure in the oxidative atmosphere, showing that single-shell graphitic allotropes such as fullerenes, graphene, and single-walled CNTs (SWCNTs) cannot resist the oxidative stress at 300°C and combust within hours. A heterogeneous model catalyst providing solely the nucleophilic diketonic carbonyl groups[7] (Fig. S3), also shows a low selectivity to the desired acid. When referred to the number of ketonic and phenolic oxygenated sites, which decompose to CO at 650–850°C as determined by temperature-programmed desorption (TPD) of the active catalysts (Tab. S2), reaction rates of 6.8×10^{-5} s^{-1} and 1.9×10^{-4} s^{-1} can be estimated for the graphite and the MWCNT catalyst, respectively, i.e., the oxygen functionalities located at the edges and defects of the curved graphene layer have a higher intrinsic activity than those terminating the flat (0001) surface. Furthermore, the bent structure induces a remarkable rise in AA selectivity. A pronounced charge location as a consequence of curvature benefits the adsorption and activation of dioxygen and may control the type of formed surface species to favour the selective turnover. On the planar basal plane the unselective peroxo species as the intermediate of O_2 adsorption with step-wise charge transfer (Eq. 2) will be more stable as compared to the epoxy group, which is the product of dissociation as favoured over the curved basal plane due to pronounced charge localization.

$$O_2(g) \rightarrow O_2(s) \rightarrow O_2^-(s) \rightarrow O_2^{2-}(s) \rightarrow O^-(s) \rightarrow O^{2-}(s) \quad (2)$$

The interaction and activation of small molecules such as O_2, H_2O, CO, or CO_2 with the defective (0001) surface has been theoretically described.[19] However, a higher degree of sp^3 hybridization as present in the active carbon and nanodiamond samples is detrimental to the AA selectivity. The moderate performance of fishbone-like carbon nanofibers (CNFs), which solely expose the prismatic edges to the outer tubular surface, further highlights the importance of extended areas of the (0001) basal plane for the reaction. The relatively poor performance of the quinone model catalyst (MCT, *m*acro*c*yclic *t*rimer) as compared to its superiority over other nanocarbon catalysts in the ODH of ethylbenzene[7] is in line with these results and gives rise to the question if the presence of nucleophilic (di)carbonyl oxygen atoms is sufficient also for the selective oxidation of C_3H_4O to AA. The stability of the catalytic system is confirmed by the 120 h long-term run and high-resolution transmission electron microscopy

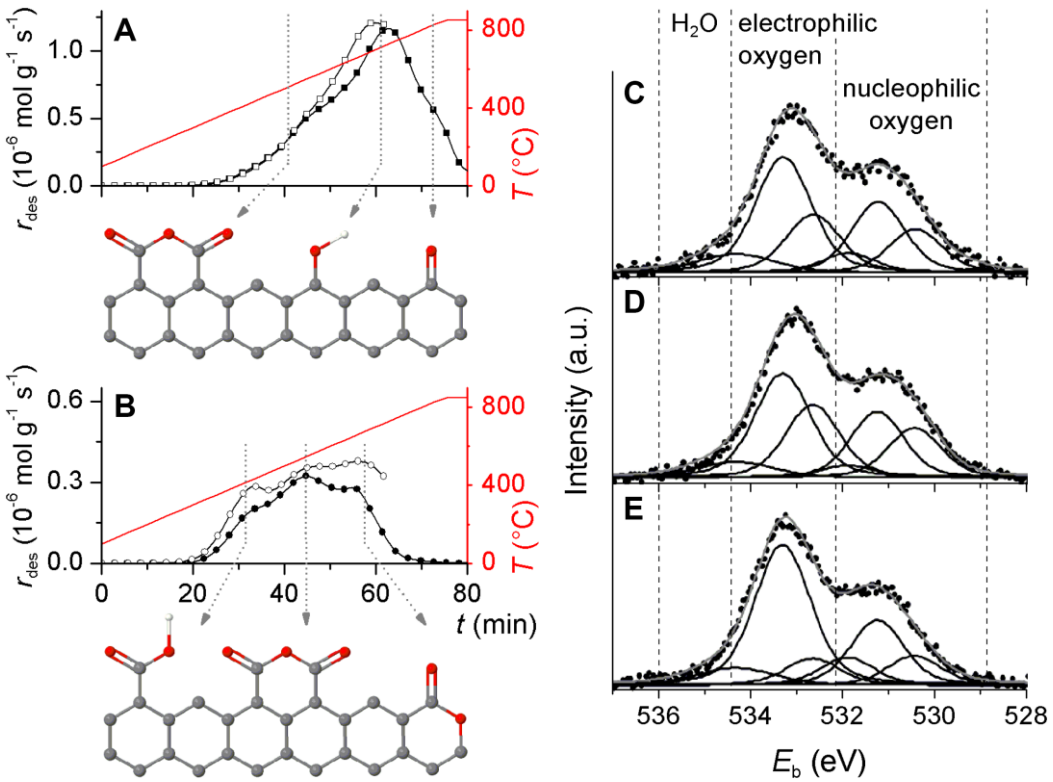

Figure 1. Surface analysis of used catalysts. (**A**) CO desorption from MWCNTs indicating the presence of anhydrides (500 ± 120°C), phenols (610 ± 120 °C), and ketones/quinones (830 ± 150°C). (**B**) CO_2 desorption from MWCNTs indicating the presence of carboxylic acids (270 ± 170°C), anhydrides (490 ± 120 °C), and lactones (700 ± 110°C).[3] The MWCNTs were pretreated for 15 h at 300 °C in a stream of 5 vol.% C_3H_4O/10 vol.% O_2/He, then cooled in He to 100 °C. The TPD profile (full symbols) was recorded at a heating rate of 10 K min^{-1} (red lines). The experiment was repeated under wet conditions (open symbols), i.e., 5 vol. % H_2O was added to the reactant/carrier gas during the pretreatment, cooling, and TPD, respectively. The functionalized surface termination is illustrated below the TPD profiles, respectively. Carbon, grey; oxygen, red; hydrogen, white. (**C** to **E**) Synchrotron-excited quasi in-situ XP spectra (O1s range) of (**C**) synthetic graphite and MWCNTs ((**D**), dry; (**E**) wet).

(HRTEM) and Raman spectroscopy analyses of used catalysts (Fig. S4) showing the structural integrity and absence of severe surface damage of the most promising MWCNT catalyst. Following the industrial process conditions we added 5 vol.% H_2O to the reaction mixture. For the MWCNTs the C_3H_4O conversion increases from 14% without addition of H_2O up to 19% in the presence of H_2O. In parallel, the AA selectivity also increases from 85 to 87%. A further increase of the steam content up to 40% drives C_3H_4O conversion and AA selectivity to 24% and 90%, respectively. The improvement of the catalytic performance is related to the modified surface properties of the carbon surface under wet conditions. TPD analyses of the catalysts clearly reveals an increased amount of carboxyl species when switching from the dry to the wet feed (Figs. 1A and B), whereas the amount of other oxygen surface species remains fairly constant. A similar result is obtained by quasi in-situ XPS (Figs. 1C to E) according to the band assignment based on literature [15], where the carboxyl band is located at around 533.0 to 533.5 eV. Accordingly, the C1s range (fig. S5) is characterized by bands at 286 and 288.5 eV indicating C–O single and C=O double bonds, respectively, as part of the surface functional groups. Their intensity is higher in the MWCNT catalysts and lower in the graphite catalyst.

This conclusively proves the impact of surface acidity, which is similarly discussed in literature for metal oxide catalysts.[13,20] Water molecules transform Lewis acid sites into Brönstedt acid centres, thus ultimately blocking the centres of total oxidation. The surface protonation further enables the formation of AA from the acrylate surface complex and additional steam favours its desorption by competitive adsorption on the catalyst surface. A shift of the phenol decomposition peak from 725 to 690°C is the most obvious change in the CO desorption profile (Fig. 1A). The destabilization of these species, which likely represent the reduced state of the red-ox active site, will likely affect their reactivity with oxygen. The positive effect of water on the catalyst reoxidation[15,21] is in line with a number of similarities between metal oxide and carbon based catalysts.

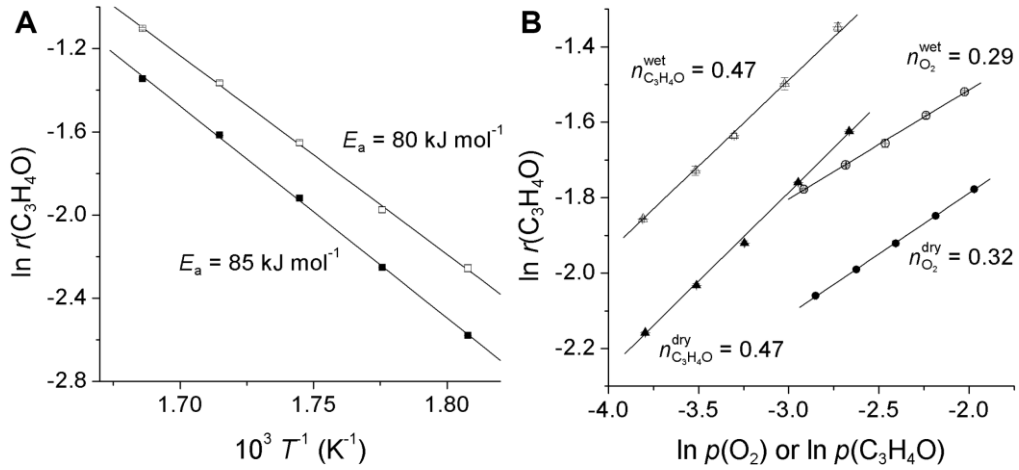

Figure 2. Reaction kinetics of C_3H_4O oxidation. (**A**) Arrhenius plot for the reaction rates under dry (full square symbols) and wet (open square symbols) conditions in the temperature range of 280 to 320°C with a gas feed of 5 vol.% C_3H_4O/10 vol.% O_2/He. (**B**) C_3H_4O oxidation rate as a function of O_2 (circle symbols) or C_3H_4O (triangle symbols) partial pressure p over MWCNTs under dry (full symbols) and wet (open symbols) conditions. The reaction rates were measured at 300°C. Wet reaction conditions were obtained by adding 5 vol.% H_2O to the reaction gas mixture.

The steady state isotopic tracer kinetic analysis (SSITKA, Fig. S6) by switching the $^{16}O_2$ oxidant to $^{18}O_2$ reveals the vital exchange of oxygen in the acrolein molecule suggesting the reversible formation of an acetal-like adsorbate on the carbon surface, whose participation as an intermediate in the selective oxidation remains rather unclear. However, this results in the formation of singly and doubly labelled AA. Again, this effect is well known to occur over Mo/V catalysts.[14] Subsequent TPD analysis of the $^{18}O_2$ treated MWCNT catalyst (Figs. S6c and d) identifies O atoms being responsible for substrate oxygenation. The exchange of $^{18}O/^{16}O$ is observed in the low temperature range of CO and CO_2 desorption, whereas the high temperature range is dominated by $C^{16}O_x$. It suggests that the nucleophilic ketones and quinones, as well as phenols as their reduced counterparts, are not removed during the redox cycle of selective C_3H_4O oxidation, in contrast to ODH catalysis operating at somewhat higher temperature.[22] Indeed, the temperature-programmed reaction of C_3H_4O with the oxygen-treated MWCNTs yields only a low amount of AA (7.3 μmol g^{-1}, Fig. S7), which is in the range of the amount released by He-TPD (7.8 μmol g^{-1}), proving that the highly stable ketones (1.4 mmol g^{-1}) will not serve the oxygen uptake of the substrate molecule. Instead labile electrophilic oxygen atoms likely insert into the formyl C–H bond after its activation by nucleophilic oxygen species. Regarding the fact that high activity/ selectivity of carbon allotropes is strictly correlated to the exposition of the (0001) basal plane to the outer surface, we suggest the mobile epoxide C–O–C species as the electrophilic product of dissociative O_2 adsorption[16,23] to be responsible for selective turnover. These are equipped with a high reactivity as a result of severe strain because the two incorporated carbon atoms change their configuretion from a planar sp^2- to a distorted sp^3-hybridized geometry. Indeed, the graphitic epoxide can migrate to the prismatic edges,[16,23] where catalytic transformation takes place, or instead, transform to more stable groups (including gasification) even at temperatures as low as 200°C.[24] The insertion of epoxide oxygen, which is present in graphene oxide, into organic molecules is indicated in a recent report[25] demonstrating the removal of epoxide in the oxidation process of benzyl alcohol in the absence of O_2. The removability of such species leaving the intact (0001) basal plane has further been predicted at least for the reaction of epoxides with adsorbed hydrogen to hydroxyl radicals and/or water.[26]

To localize the active sites at the prismatic edges, we modified the surface of MWCNTs with 1 wt.% B_2O_3 and P_2O_5, respectively. It is reported, that these heteroatoms selectively block the zigzag and armchair terminations of graphene sheets, respectively.[27] The decreased C_3H_4O conversions of 6.5% for the B_2O_3/MWCNTs and 5.2% for the P_2O_5/MWCNTs thus evidence the catalytic activity of both configurations. However, the P modification results in an increased AA selectivity of 90.9% over the pristine MWCNTs, whereas the B modified sample shows a lower AA selectivity of 83.9%. It suggests that the quinone group located at the zigzag termination of the graphene layer acts more selective in the C_3H_4O oxidation than the one in armchair configuration, even though this effect is only weakly pronounced. It should also be considered that this kind of modification also affects the surface acidity and blocks point defects. The robustness of the catalytic system is unique: neither (short-term) harsh oxidative stress nor high-temperature calcination, which substantially defunctionalizes the carbon surface, can induce persistent damage to its catalytic function. The CNT catalyst rapidly recovers after treatment in air at 500°C as well as after TPD in He up to 850°C and the catalyst approaches its initial activity and

selectivity within a few hours (Fig. S8). As compared to metal oxide catalysts often comprising several more or less active and selective crystallographic phases, which may transform into each other in the course of reaction and cause irreversible deactivation, the graphitic carbon is the thermodynamically most favourable form of carbon thus providing no point of attack for structural rearrangement.

The variation of gas-hourly space velocity (GHSV) reveals a weakly decreasing AA selectivity as the C_3H_4O conversion increases up to 15% (Fig. S9), suggesting that the formation of CO_x, the only by-products observed, occurs via direct C_3H_4O combustion, whereas AA is more resistant to total oxidation. In contrast to O_2, the H_2O concentration has major impact on the product distribution. Thus, the impact of H_2O on the reaction was investigated also by kinetic analysis. The preexponential factor remains fairly constant at around $(3 \pm 1) \times 10^{24}$ molecules g^{-1} s^{-1} indicating that the number of active sites will not change when switching from the dry to the wet feed. However, addition of 5% H_2O to the reactant gas mixture significantly lowers the apparent activation energy from 85 to 80 kJ mol^{-1} (Fig. 2A). The lowering of the barrier must be referred to the surface acidity induced by surface carboxyl groups which likely affect the reactant adsorption and/or the transition state of the C_3H_4O selective oxidation reaction mechanism. The activation energy under dry conditions fits the barrier of epoxy group hopping (0.9 eV) as determined by first principles calculations,[23] suggesting that oxygen mobility on the (0001) graphitic surface might be the rate determining factor of the reaction. This is plausible if we consider the reaction to occur at the edge of the basal planes of CNTs. A moderate impact of catalyst reoxidation on the overall rate is confirmed by a kinetic isotope effect (KIE) of $k(^{16}O_2)/k(^{18}O_2) = 1.06$ (Fig. S6b). The reaction orders of C_3H_4O and O_2 over the MWCNTs under dry conditions are 0.47 and 0.32 (Fig. 2B), respectively. Broken rate orders agree with the multi-step reaction mechanism and indicate that the carbon surface is almost saturated with C_3H_4O and/or AA and the limitation of the reaction rate holds the balance between the surface reaction of C_3H_4O with the oxidized carbon surface, the catalyst reoxidation, and by the desorption of AA from the active site. The conjugated π-electrons of substrate and reaction product molecules can favour their adsorption on the (0001) basal plane by van-der-Waals forces. The reaction order of C_3H_4O keeps constant in the presence of 5% H_2O suggesting that the hydrocarbon activation is not affected. Against that, the decrease of the rate order of O_2 to 0.29 can likely be interpreted with the accelerated reoxidation of the carbon surface by the addition of steam, which has also been observed for the combustion of graphitic carbon as well as for the oxidation of VO_x clusters supported on γ-Al_2O_3.[15,21] Taking all these experimental results and theoretic background into account the following pathway for C_3H_4O oxidation is suggested (Fig. 3).

In conclusion, the element carbon was demonstrated to be a highly robust and selective catalyst for a chemical model reaction with oxygen insertion into an organic molecule. In the selective oxidation of acrolein, an acrylic acid productivity of 26.5 mmol g^{-1} h^{-1} could be achieved, which is almost half as high as for the industrial doped MoV mixed oxide (about 60 mmol g^{-1} h^{-1}).[12] Fundamental structure-activity relationships could be established to optimize the catalytic performance with respect to the carbon microstructure and reaction conditions, respectively. Such a morphological control in a macroscopic scale is difficult to achieve for metal (oxide) catalysts,[28] thus giving elemental carbon a unique position in catalysis science. In general, carbon catalysis in the absence of polyvalent metal sites with complex electronic and spin structures, allows for facile and in-depth theoretical analysis and thus is an ideal model for the understanding of reaction mechanisms. In the present study, the reaction mechanism of selective C_3H_4O oxidation could be clarified in substantial parts by highlighting the importance of nucleophilic and electrophilic oxygen species, the prismatic edges as well as the basal planes of graphite, and the abundance of protons being delivered either by carboxyl groups or by water. Important input from ab-initio calculations available for the graphene model is an independent basis for the interpretation of experimental data. We could identify substantial similarities between the metal oxide and the carbon catalyzed reaction, which might help to bridge the gap between these apparently incompatible catalytic systems.

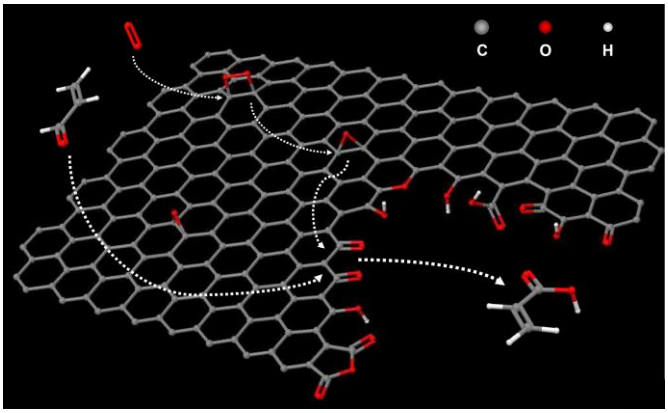

Figure 3. Suggested reaction pathway for C_3H_4O oxidation at the graphitic carbon surface. The active domain is illustrated as a rectangular section of a planar graphene sheet with a hole defect, which is terminated by arbitrarily positioned oxygen functionalities. O_2 adsorbs dissociatively at the (0001) surface to form mobile epoxy groups, which migrate to the prismatic edge sites located at the ends and surface defects of MWCNTs. The adsorption of C_3H_4O at the nucleophilic oxygen sites, i.e., the ketones/quinones, initiates its oxygenation by epoxy oxygen atoms to acrylic acid.

Experimental Section

Catalytic testing: Sample amounts of 500 mg (100–300 µm) were tested in a fixed bed quartz reactor under atmospheric pressure. The reactor was heated with 5 K min^{-1} up to 300°C and the feed compri–sing of 5% C_3H_4O, 10% O_2, 0–5% H_2O, and balance He was dosed by mass-flow controllers (O_2, He) and saturators (H_2O, C_3H_4O) at a total flow of 25 ml min^{-1} (GHSV of 3000 h^{-1}). Kinetic measurements were conducted at 275–325°C with feed streams of 2-10% C_3H_4O and 5-20% O_2 balanced with He. Differential conditions were ensured by an increased total flow of 100 ml min^{-1} resulting in C_3H_4O conversions of < 5%. Reactants and products in the inlet and outlet streams were

quantified by an on-line gas chromatograph (Varian CP-4900).

Structural characterization: HRTEM analyses were recorded on a Philips CM 200 LaB6 microscope at an acceleration electron voltage of 200 kV. The specimens were prepared by suspension of the nanocarbon powder in ethanol. Drops of the suspensions were deposited on carbon-enhanced C grids and dried in air. Laser Raman spectroscopy was performed on powder samples by using an ISA LabRam instrument equipped with an Olympus BX40 microscope. The excitation wavelength was 632.8 nm and a spectral resolution of 0.9 cm^{-1} was used. Specific surface areas were determined by N_2 physisorption at –196°C and calculated from the adsorption branch in the range of p/p_0 = 0.05–0.3 by the method of Brunauer, Emmet, and Teller (BET). For XPS and TPD analyses the MWCNTs catalyst samples were cooled down to ambient in the dry and wet feed, respectively. For TPD the sample was directly subjected to a temperature ramp (10 K min^{-1}) in 25 ml min^{-1} of He. The molecules released from the surface by desorption and/or decomposition of surface species up to 850°C were quantified by an on-line mass spectrometer and an on-line gas chromatograph, respectively. Synchroton-excited XPS analyses were performed at the ISISS beamline at BESSY II. The compressed sample tablets were analyzed under quasi in-situ conditions in UHV at a temperature of 300°C.

References

[1] a) S. Iijima, *Nature* **1991**, *354*, 56-58; b) H. W. Kroto, J. R. Heath, S. C. O'Brien, R. F. Curl, R. E. Smalley, *Nature* **1985**, *318*, 162-163.
[2] K. S. Novoselov, A. K. Geim, S. V. Morozov, D. Jiang, Y. Zhang, S. V. Dubonos, I. V. Grigorieva, A. A. Firsov, *Science* **2004**, *306*, 666-669.
[3] P. Serp, J. L. Figueiredo, *Carbon Materials for Catalysis*, John Wiley & Sons, **2009**.
[4] K. P. De Jong, J. W. Geus, *Catal. Rev. - Sci. Eng.* **2000**, *42*, 481.
[5] D. R. Dreyer, C. W. Bielawski, *Chem. Sci.* **2011**, *2*, 1233.
[6] a) H.-P. Jia, D. R. Dreyer, C. W. Bielawski, *Tetrahedron* **2011**, *67*, 4431-4434; b) H.-P. Jia, D. R. Dreyer, C. W. Bielawski, *Adv. Synth. Catal.* **2011**, *353*, 528-532; c) D. R. Dreyer, S. Murali, Y. Zhu, R. S. Ruoff, C. W. Bielawski, *J. Mater. Chem.* **2011**, *21*, 3443; d) D. R. Dreyer, S. Park, C. W. Bielawski, R. S. Ruoff, *Chem. Soc. Rev.* **2010**, *39*, 228.
[7] J. Zhang, X. Wang, Q. Su, L. Zhi, A. Thomas, X. Feng, D. S. Su, R. Schlögl, K. Müllen, *J. Am. Chem. Soc.* **2009**, *131*, 11296-11297.
[8] J. Zhang, D. S. Su, A. Zhang, D. Wang, R. Schlögl, C. Hébert, *Angew. Chem. Int. Ed.* **2007**, *46*, 7319–7323.
[9] J. Zhang, D. S. Su, R. Blume, R. Schlögl, R. Wang, X. Yang, A. Gajović, *Angew. Chem. Int. Ed.* **2010**, *49*, 8640-8644.
[10] a) B. Frank, J. Zhang, R. Blume, R. Schlögl, D. S. Su, *Angew. Chem. Int. Ed.* **2009**, *48*, 6913–6917; b) X. Liu, B. Frank, W. Zhang, T. P. Cotter, R. Schlögl, D. S. Su, *Angew. Chem. Int. Ed.* **2011**, *50*, 3318–3322; c) B. Frank, M. Morassutto, R. Schomäcker, R. Schlögl, D. S. Su, *ChemCatChem* **2010**, *2*, 644–648.
[11] Hodnett, B.K., in *Supported Catalysts and Their Applications* (Eds.: Sherrington, D.C., Kybett, A.P.), RSC, **2001**, pp. 1-8.
[12] T. Ohara, T. Sato, N. Shimizu, G. Prescher, H. Schwind, O. Weiberg, K. Marten, H. Greim, in *Ullmann's Encyclopedia of Industrial Chemistry*, Wiley VCH, Weinheim, Germany, **2003**.
[13] J. Tichý, *Appl. Catal. A* **1997**, *157*, 363-385.
[14] P. Kampe, L. Giebeler, D. Samuelis, J. Kunert, A. Drochner, F. Haa?, A. H. Adams, J. Ott, S. Endres, G. Schimanke, et al., *Phys. Chem. Chem. Phys.* **2007**, *9*, 3577.
[15] B. Frank, A. Rinaldi, R. Blume, R. Schlögl, D. S. Su, *Chem. Mater.* **2010**, *22*, 4462–4470.
[16] R. T. Yang, C. Wong, *Science* **1981**, *214*, 437-438.
[17] M. Sadakane, N. Watanabe, T. Katou, Y. Nodasaka, W. Ueda, *Angew. Chem. Int. Ed.* **2007**, *46*, 1493-1496.
[18] O. Shenderova, V. Zhirnov, D. Brenner, *Crit. Rev. Solid State Mater. Sci.* **2002**, *27*, 227-356.
[19] a) M. K. Kostov, E. E. Santiso, A. M. George, K. E. Gubbins, M. B. Nardelli, *Phys. Rev. Lett.* **2005**, *95*, 136105; b) S. M. Lee, Y. H. Lee, Y. G. Hwang, J. R. Hahn, H. Kang, *Phys. Rev. Lett.* **1999**, *82*, 217; c) S. C. Xu, S. Irle, D. G. Musaev, M. C. Lin, *J. Phys. Chem. C* **2009**, *113*, 18772-18777.
[20] T. V. Andrushkevich, *Catal. Rev. - Sci. Eng.* **1993**, *35*, 213.
[21] B. Frank, R. Fortrie, C. Hess, R. Schlögl, R. Schomäcker, *Appl. Catal. A* **2009**, *353*, 288-295.
[22] J. Zhang, X. Liu, R. Blume, A. Zhang, R. Schlögl, D. S. Su, *Science* **2008**, *322*, 73-77.
[23] J.-L. Li, K. N. Kudin, M. J. McAllister, R. K. Prud'homme, I. A. Aksay, R. Car, *Phys. Rev. Lett.* **2006**, *96*, 176101.
[24] H.-K. Jeong, Y. P. Lee, M. H. Jin, E. S. Kim, J. J. Bae, Y. H. Lee, *Chem. Phys. Lett.* **2009**, *470*, 255-258.
[25] D. R. Dreyer, H.-P. Jia, C. W. Bielawski, *Angew. Chem. Int. Ed.* **2010**, *49*, 6813-6816.
[26] A. Jelea, F. Marinelli, Y. Ferro, A. Allouche, C. Brosset, *Carbon* **2004**, *42*, 3189-3198.
[27] C. Park, R. T. K. Baker, *J. Phys. Chem. B* **1999**, *103*, 2453-2459.
[28] a) X. Xie, Y. Li, Z.-Q. Liu, M. Haruta, W. Shen, *Nature* **2009**, *458*, 746-749; b) A. Celaya Sanfiz, T. W. Hansen, A. Sakthivel, A. Trunschke, R. Schlögl, A. Knoester, H. H. Brongersma, M. H. Looi, S. B. A. Hamid, *J. Catal.* **2008**, *258*, 35-43.